DALTON
FULL PAPER

Azulenylium and guaiazulenylium cations as novel accepting moieties in extended sesquifulvalene type D–π–A NLO chromophores †

Tony Farrell,*[ab] Timo Meyer-Friedrichsen,[b] Maik Malessa,[b] Detlev Haase,[c] Wolfgang Saak,[c] Inge Asselberghs,[d] Kurt Wostyn,[d] Koen Clays,[d] André Persoons,[d] Jürgen Heck *[b] and Anthony R. Manning *[a]

[a] *University College Dublin, Belfield, Dublin 4, Ireland*
[b] *Institut für Anorganische und Angewandte Chemie, Universität Hamburg, Martin-Luther-King-Platz 6, D-20146 Hamburg, Germany*
[c] *Universität Oldenburg, FB Chemie, Carl-von-Ossietzkystr. 9–11, 26111 Oldenburg, Germany*
[d] *Laboratorium voor chemische en biologische dynamica, Katholieke Universiteit Leuven, Celestijnenlaan 200D, B-3001 Leuven, Belgium*

Received 14th August 2000, Accepted 31st October 2000
First published as an Advance Article on the web 13th December 2000

The novel series of monometallic monocations Fc-[*n*]-Az^+ and Fc-[*n*]-$Guaz^+$ (where Az^+ and $Guaz^+$ denote azulenylium and guaiazulenylium cations respectively and $n = 0$–3), and a bimetallic dicationic complex Fc-[0]-$Guaz(RuCp)^{2+}$ have been prepared. Single crystal structures of Fc-[0]-$Guaz^+$ and Fc-[0]-$Guaz(RuCp)^{2+}$ have been determined. Analysis of the bond lengths and angles coupled with the electrochemistry data provides evidence for strong ground state charge transfer in the series which diminishes upon π-bridge extension. The electronic absorption spectra reveal that alkylation of the cationic terminus (1) diminishes the electron-accepting ability, (2) results in a larger dipole moment change upon excitation and (3) causes a smaller sequential lowering of the CT transitions with π-bridge extension. The NLO properties which were characterised by hyper-Rayleigh scattering techniques indicate the potential of the azulenylium based donor–acceptor chromophores, but also that the extended complexes exhibit two-photon absorption fluorescence.

Introduction

A major feature of the research into materials capable of doubling the frequency of incident light (second harmonic generation (SHG)), a second order non-linear optical (NLO) property, is the determination of the first hyperpolarisability β. The most important class of compounds capable of frequency doubling are formed by an electron donor (D), an acceptor (A) and a π bridge providing the electronic pathway between the donor and acceptor. Our interest is in the design of D–π–A systems with one or both organometallic termini.

A simplified and commonly used theoretical model to relate β to the molecular electronic properties is the two-level model (TLM).[1] This approach takes into account the ground state and one excited state *e.g.* the charge-transfer (CT) state, which have different polarities, eqns. (1) and (2), where $\Delta\mu_{eg}$ is the change in

$$\beta_{CT}(-2\omega,\omega,\omega) = \frac{3\Delta\mu_{eg}M^2}{(\hbar\omega_{eg})^2} \cdot \frac{\omega_{eg}^2}{(1 - 4\omega^2/\omega_{eg}^2)(\omega_{eg}^2 - \omega^2)} \quad (1)$$

$$\beta_0 = 3\Delta\mu_{eg}M^2/(\hbar\omega_{eg})^2 \quad (2)$$

the dipole moment between the ground and the CT state, M the electronic transition moment, $\hbar\omega_{eg}$ the energy of the optical transition between the ground and CT state (in a simplified model the electronic excitation from the HOMO to the LUMO), ω_{eg} the circular frequency of the optical transition, ω the fundamental circular frequency of the incident radiation and β_0 the frequency independent first hyperpolarisability. Eqn. (1) predicts that large, frequency independent first hyperpolarisabilities are obtained for compounds undergoing a low energy CT transition ΔE_{eg}, a large transition moment M which is directly correlated to the oscillator strength or in other words the absorption coefficient ε should be large,[2] a large change in dipole moment $\Delta\mu_{eg}$, which is indicated by a pronounced solvatochromism of the CT transition.[3]

The special features of metal coordinated donors and acceptors have been well documented,[4] and ferrocenyl chromophores possess some of the largest microscopic and macroscopic second order non-linearities reported to date for organometallic compounds.[5] Conventional methods of enhancing β for D–π–A systems include increasing the electron acceptor strength and extending the conjugation pathway. However, we have found that elongation of the π bridge in sesquifulvalene type complexes leads to a decrease in ground state (GS) communication between the termini and a "slowing" of the lowering of energy of the charge transfer (CT) band.[5a] Simply said, the DA-CT energy reaches a limiting value for an increasing number of double bonds between the donor and acceptor moieties. This property reflects the characteristic feature of merocyanines which demonstrate a distinct bond length alternation (BLA) in the olefinic bridge; the bathochromic shift decreases faster when the BLA is more pronounced.[6]

Azulene and its alkylated derivatives are quite unique in that the disruption of aromaticity on going from the neutral form is counterbalanced by the gain of resonance energy upon formation of the azulenylium carbocation (Fig. 1).[7] Therefore,

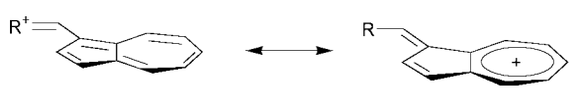

Fig. 1 Resonance forms of a substituted azulenylium carbocation.

† Dedicated to Professor Dr Henry Brunner on the occasion of his 65th Birthday.

DOI: 10.1039/b006624i

as a consequence of this aromatic stabilisation in both the neutral and charge-separated forms, azulene and its alkylated derivatives can act as extremely potent electron donors and acceptors. In comparison with conventional organic donors such as disubstituted *p*-*N*,*N*-dimethylaminoaniline, which loses resonance stabilisation upon charge separation, and strong electron acceptors, for example thiobarbituric acid which only gains aromatic stabilisation upon charge separation, azulene appears to be an extremely novel and interesting system. Surprisingly, there are very few reports to date of azulene NLO chromophores and X-ray data are even more sparse.[8] Herein, we present the facile combination of ferrocene with azulenylium based carbocations as electron acceptors.

Results and discussion

Synthesis

The formyl ferrocene precursors were afforded in high yields by the preparatively convenient method of Spangler and McCoy (Scheme 1).[9] The known ferrocenyl carbaldehydes were

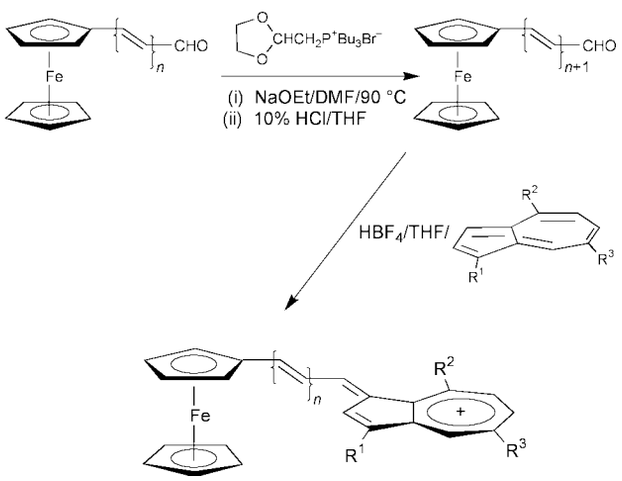

Scheme 1 Synthesis of vinylogue formyl ferrocenes and the corresponding azulenylium carbocations. Fc-[*n*]-Az$^+$: $R^1 = R^2 = R^3 = H$; $n = 0$–2; azulenylium carbocations. Fc-[*n*]-Guaz$^+$: $R^1 = R^2 = Me$, $R^3 = i$-Pr; $n = 0$–2; guaiazulenylium carbocations.

characterised by ^{1}H NMR and exhibited signals which were consistent with all *trans* geometry. The ferrocene azulenylium (Fc-[0]-Az$^+$) and guaiazulenylium (Fc-[0]-Guaz$^+$) carbocations are readily available *via* condensation of the azulene species with the formyl ferrocene in the presence of HBF_4 (Scheme 1) or HPF_6.[10]

The ruthenated dicationic complex Fc-[0]-Guaz(RuCp)$^{2+}$ was effectively formed by the reaction of Fc-[0]-Guaz$^+$ with one equivalent of [RuCp(MeCN)$_3$][PF$_6$][11] in CH_2Cl_2 (Scheme 2).

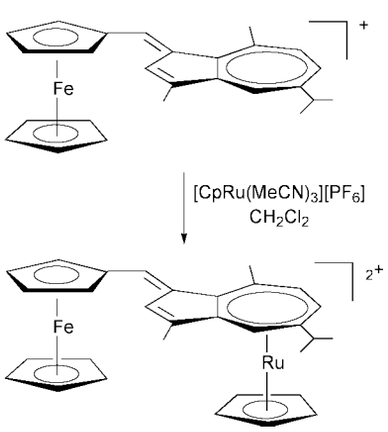

Scheme 2 Synthesis of Fc-[0]-Guaz(RuCp)$^{2+}$.

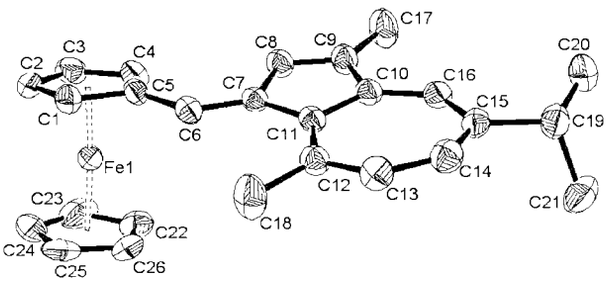

Fig. 2 Thermal ellipsoid plot of the Fc-[0]-Guaz$^+$ cation (50% probability; hydrogens, solvent molecule and BF_4 counter ion omitted for clarity).

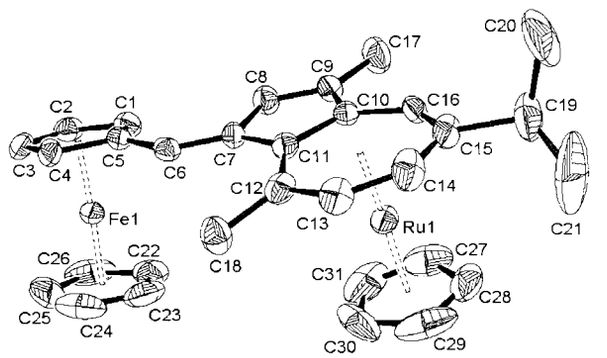

Fig. 3 Thermal ellipsoid plot of the Fc-[0]-Guaz(RuCp)$^{2+}$ cation. (Details as in Fig. 2.)

The resulting dicationic species was obtained upon concentration of the reaction mixture and washed with Et_2O. Both the $(PF_6)_2$ and the mixed counter ion $(BF_4)(PF_6)$ salts were prepared.

Crystal structures of Fc-[0]-Guaz$^+$ and Fc-[0]-Guaz(RuCp)$^{2+}$

Crystals suitable for structure determination of Fc-[0]-Guaz$^+$ were grown from a concentrated THF solution and for the Fc-[0]-Guaz(RuCp)$^{2+}$ dicationic complex from diffusion of Et_2O into a CH_3NO_2 solution of the mixed counter ion compound. However, the structure analysis was performed with a single crystal of the $(BF_4)_2$ salt. To our knowledge these are the first crystallographic structure determinations of guaiazulenylium carbocations. Views of the molecular structures are illustrated in Figs. 2 and 3 along with atom labeling while selected bond lengths and angles are listed in Table 1. The crystal structure analysis of Fc-[0]-Guaz$^+$ reveals that about 13% of the two enantiomeric forms present in the solid state of the molecule are disordered. They were separated using a disorder model giving final *R* indices (all data) of $R1 = 0.0981$ and $wR2 = 0.2290$. In particular the structure determination of Fc-[0]-Guaz(RuCp)$^{2+}$ verifies the exclusive coordination of the (RuCp)$^+$ fragment to the guaiazulenylium seven-membered ring.

Both complexes crystallise in centrosymmetric space groups and therefore solid-state NLO studies to evaluate the SHG were not carried out. Nonetheless interaction between the two π termini of D–π–A chromophores in the solid state has often been useful in indicating potential NLO active materials.[12] For ferrocenyl D–π–A systems this end-group communication, *i.e.* a more fulvene like GS structure (Fig. 4), is reflected in a lengthening of the sp^2–sp^2 carbon–carbon double bond (134 pm) proximate to the metallocene, and a concomitant bending of the alpha-carbon towards the metal.[13] These structural effects, although not very pronounced, are observable for both structures presented here and clearly indicate charge transfer in the ground state.

Within the entire molecular framework the greatest deviation from planarity is between the η^5-C_5H_4 (C1–C5) unit and the

Table 1 Selected bond lengths (pm) and angles (°) for Fc-[0]-Guaz$^+$ and Fc-[0]-Guaz(RuCp)$^{2+}$

	Fc-[0]-Guaz$^+$	Fc-[0]-Guaz(RuCp)$^{2+}$
Fe(1)–C(6)	303.8(6)	301.2(7)
C(5)–C(6)	143.9(5)	145.1(7)
C(6)–C(7)	138.3(6)	136.0(7)
C(7)–C(8)	144.8(6)	144.7(7)
C(7)–C(11)	147.4(6)	147.4(7)
C(8)–C(9)	136.3(6)	135.8(8)
C(9)–C(10)	145.1(6)	144.9(7)
C(10)–C(16)	140.8(6)	141.6(7)
C(10)–C(11)	145.4(5)	145.0(8)
C(11)–C(12)	140.8(6)	141.7(7)
C(12)–C(13)	141.9(6)	143.8(7)
C(13)–C(14)	138.3(6)	138.7(9)
C(14)–C(15)	140.8(7)	140.5(9)
C(15)–C(16)	138.7(7)	141.3(8)
Cp(1)[a]–C(5)–C(6)	173.3(3)	170.8(3)
Cp(1)[a]–[C(7)–C(16)]	17.1(2)[b]	17.5(1)[b]
Cp(1)[a]–[C(6)–C(7)–C(11)]	13.7(4)[b]	9.1(3)[b]
[C(5)–C(6)–C(7)]–[C(7)–C(11)][c]	4.1(3)[b]	6.8(1)[b]

[a] Center of the Cp ring C(4)–C(8). [b] Angle between the two planes. [c] Center of Cp ring.

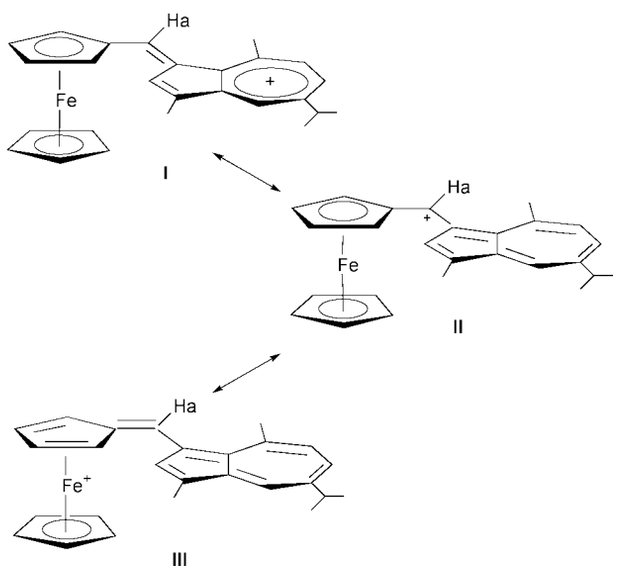

Fig. 4 Three resonance forms for the guaiazulenylium based carbocations.

guaiazulenylium moiety: 17.1(2)° for Fc-[0]-Guaz$^+$ and 17.5(1)° for Fc-[0]-Guaz(RuCp)$^{2+}$, and is effected *via* the C5–C6 single bond. Most notable is the overall planarity of the guaiazulenylium moiety with C12 (8.2(4) and 8.6(4) pm) and C14 (−7.6(4) and –5.1(5) pm) displaying greatest out of plane distortions in both structures. The reason for this we believe is to allow the guaiazulenylium methyl group to bend down below the plane in order to reduce the repulsive interaction between it and the vinylic proton (H6) in the crystal lattice. Thus if the C12–C13 and C13–C14 bond lengths are disregarded, the guaiazulenylium moiety has nearly equal bond lengths within the seven-membered ring (1.383–1.408 pm for Fc-[0]-Guaz$^+$ and 1.417–1.405 pm for Fc-[0]-Guaz(RuCp)$^{2+}$). This in conjunction with the high degree of bond length alternation in the guaiazulenylium five-membered ring emphasises the predominant localisation of the positive charge in the seven-membered ring in the solid state (structure **I** Fig. 4). As expected, the bond fusing the five- and seven-membered rings is longer than the peripheral bonds (145.0 and 145.4 pm for Fc-[0]-Guaz$^+$ and Fc-[0]-Guaz(RuCp)$^{2+}$ respectively), but distinctly shorter than the transannular bridging bond in azulene (149.8 pm)

Table 2 ^{1}H NMR data for Fc-[*n*]-Az$^+$ and Fc-[*n*]-Guaz$^+$

	Fc-[*n*]-Az$^+$				Fc-[*n*]-Guaz$^+$			
n	H_α	η^5-C_5H_5	η^5-C_5H_4		H_α	η^5-C_5H_5	η^5-C_5H_4	
0	9.35	4.57	5.79	5.54	9.04	4.51	5.44	5.40
1	8.45	4.52	5.47	5.28	8.12	4.37	5.07	
2	7.89	4.41	5.16	5.02	7.37	4.36	4.89	
3	7.45	4.32	4.91	4.86		4.21	4.69	

which is further evidence for the presence of a tropylium-like GS.

NMR Spectroscopy

The NMR data are given in Table 2 and a number of conclusions can be drawn on the ground state structure of these chromophores. First, the seven-membered ring protons are significantly shifted to lower field strengths relative to those of the parent azulene. For example, for the complex Fc-[0]-Guaz$^+$: $\Delta\delta$(H4) = 0.45, $\Delta\delta$(H6) = 0.92, $\Delta\delta$(H7) = 1.53 ppm (for numbering scheme see Experimental section), where $\Delta\delta$ denotes the difference between the chemical shifts of the carbocationic derivative and guaiazulene. This effect reflects the localisation of the positive charge in the seven-membered ring and the overall dominant contribution of the resonance form **I** (Fig. 4), to the ground state. Owing to the influence of the coordinated ruthenium fragment in Fc-[0]-Guaz(RuCp)$^{2+}$ the proton resonances of the guaiazulenylium seven-membered ring are strongly shifted upfield (>1 ppm). The protons signals of the guaiazulenylium five-membered ring and even the olefinic proton signals (proximate to the metallocene Cp, Ha, Fig. 4) also experience an upfield shift but of reduced magnitude (≈0.3 ppm).

Extension of the π bridge results in: (i) an upfield shift of the η^5-C_5H_5 and η^5-C_5H_4 ring protons, (ii) a reduction in the chemical shift difference between the two η^5-C_5H_4 ring signals and (iii) an upfield shift in the position of the proton Ha . These results can be interpreted on the basis of simple electronic effects and illustrate the degree of interaction between the cationic center and the electron rich ferrocene moiety, *i.e.* the contribution of resonance forms **II** and **III** to the GS structure (Fig. 4).

Moreover, the chemical shifts of the Ha proton and the ferrocenyl ring protons of the Fc-[*n*]-Guaz$^+$ series are consistently upfield of the corresponding signals of the Fc-[*n*]-Az$^+$ complexes. This may be regarded as a manifestation of the increased stability of the tropylium based carbocations and therefore lower electron accepting capabilities of the azulenylium terminus upon alkylation. Moreover, though not unexpectedly, the Fc-[*n*]-Az$^+$ series has increased contribution from form **III** to the overall GS configuration.

Electrochemistry

To get a deeper insight into the ground state properties and more specifically the mutual donor–acceptor electronic influence, we studied the redox properties of the complexes by cyclic voltammetry and the results are presented in Table 3. The compounds exhibit an electrochemically reversible one-electron oxidation half wave potential ($E_{\frac{1}{2}}$) which is positively shifted with respect to that of ferrocene. Communication between the electron donating and accepting termini can be evaluated by comparing the $E_{\frac{1}{2}}$ values. A more positive half wave potential, suggests that the ferrocene unit is more difficult to oxidise (*i.e.* less electron rich). The extent of this interaction is highly dependent on the length of the π bridge, *i.e.* as the separation of the termini increases through insertion of double bonds $E_{\frac{1}{2}}$ approaches that of ferrocene itself. The differences in the $E_{\frac{1}{2}}$ potentials between the Fc-[*n*]-Az$^+$ and Fc-[*n*]-Guaz$^+$ derivatives reflect the electron accepting capabilities of the

Table 3 Electrochemical data[a] for Fc-[*n*]-Az^+ and Fc-[*n*]-$Guaz^+$

	Fc-[*n*]-Az^+			Fc-[*n*]-$Guaz^+$		
n	$E_{1/2}$[a]/V	E_{pc}[b]/V	ΔE/V	$E_{1/2}$[a]/V	E_{pc}[b]/V	ΔE/V
0	0.35	−0.80	1.15	0.31	−0.90	1.21
1	0.25	−0.77	1.02	0.17	−0.88	1.05
2	0.16	−0.65	0.81	0.10	−0.81	0.91
3	0.08	−0.63	0.71	0.05	−0.76	0.81
Fe-[0]-Guaz$(RuCp)^{2+}$				0.50	−0.42	0.92

[a] In CH_2Cl_2 *vs.* $[FeCp_2]$–$[FeCp_2]^+$. [b] Irreversible one electron reduction.

Table 4 Linear and non-linear optical data

	λ_{max}/nm [ε/M^{-1} cm^{-1}][a]		$\Delta\nu$[b]/cm^{-1}			
Compound	DA-CT	LL-CT	DA-CT	LL-CT	β[c]/10^{-30} esu	β_0/10^{-30} esu
Fc-[0]-Az^+	716 (10 200)	474 (18 100)	−340	−689	326	145
Fc-[1]-Az^+	798 (17 300)	552 (29 100)	−592	−403	—	—
Fc-[2]-Az^+	866 (22 900)	616 (31 100)	−906	−573	810[d]	451
Fc-[3]-Az^+	920 (35 900)	666 (34 900)	−951	−909	—	—
Fc-[0]-$Guaz^+$	724 (13 500)	474 (22 400)	−474	−548	220	101
Fc-[1]-$Guaz^+$	782 (21 600)	540 (31 800)	−744	−975	1539[d]	821
Fc-[2]-$Guaz^+$	827 (35 400)	587 (42 200)	−1066	−1015	1373[d] (360)[e]	770 (132)[e]
Fc-[3]-$Guaz^+$	859 (43 300)	619 (43 600)	−1488	−680	—	—
Fc-[0]-Guaz$(RuCp)^{2+}$[f]	698 (17 200)	452 (29 600)	−208	−1396	326	134

[a] In CH_2Cl_2. [b] $\Delta\nu = \nu_{max}(CH_2Cl_2) - \nu_{max}(CH_3CN)$. [c] In CH_2Cl_2, $\lambda = 1064$ nm. [d] TPAF enhanced. [e] Obtained from high frequency demodulation at $\lambda = 1300$ nm. [f] The $(PF_6)_2$ salt was used.

cationic fragments. Alkylation of the seven-membered ring of the azulenic terminus results in a more stable tropylium based carbocation and the $E_{\frac{1}{2}}$ potentials correspond to the change in electron density at the electron donating metallic terminus. Moreover, comparing the oxidation potentials of Fc-[0]-Az^+ ($E_{\frac{1}{2}} = 0.35$ V) and Fc-[0]-$Guaz^+$ ($E_{\frac{1}{2}} = 0.31$ V) with that of the electronically related ferrocenyltropylium complex $[Fe(\eta^5\text{-}C_5H_5)(\eta^5\text{-}C_5H_4CH{=}CHC_7H_6)][PF_6]$[5a] ($E_{\frac{1}{2}} = 0.22$ V) reveals greater GS electronic communication between the azulenylium based acceptors and the ferrocenyl termini than between the tropylium and ferrocene units.

In contrast, the reduction of the series occurs in an irreversible one-electron transfer. The data illustrate that there is quite an obvious electrochemical distinction between the compounds depending on the π-linker length and alkylation at the cationic terminus. Thus alkylation and decreased donor–acceptor separation results in an increased negative shift of the reduction potential E_{pc}.

Nonetheless, it should be noted that the HOMO is essentially ferrocene based while the character of the LUMO is dominated by the cationic azulenylium. These characteristics suggest charge transfer from the ferrocene to the azulenylium cation upon excitation. The decrease in energy of the HOMO–LUMO gap upon π-bridge extension is illustrated by the lowering of the ΔE value, the difference between the oxidation ($E_{\frac{1}{2}}$) and reduction potentials (E_{pc}).

Electronic absorption spectroscopy

The UV-vis spectral data are presented in Table 4 and are consistent with most ferrocenyl chromophores in that they exhibit two charge-transfer bands in the visible region.[14] As in our previous works[5a,13b,15a] and in agreement with the latest theoretical treatment,[15b] we assign the lower energy band to a donor–acceptor charge-transfer (DA-CT) transition and the higher lying absorption as an interligand π–π* transition (LL-CT).

Fig. 5 demonstrates the influence of the π-bridge length on both bands for the Fc-[*n*]-Az^+ series. As is the case in many other reported ferrocenyl series, the red-shift is greater for the higher-energy absorption while the shift to lower energies for

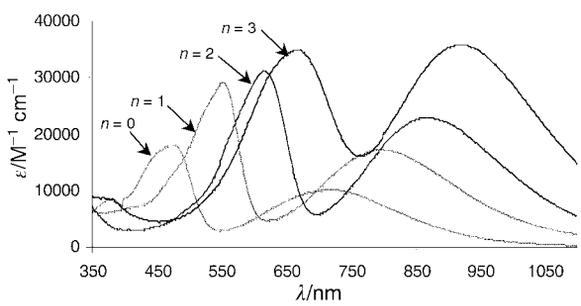

Fig. 5 UV-vis spectra of the Fc-[*n*]-Az^+ series demonstrating the effect of the conjugated bridge on absorption maxima.

the DA-CT band has quickly reached the merocyanine limit of the system. For example, for the related ferrocenyltropylium complexes $[Fe(\eta^5\text{-}C_5H_5)(\eta^5\text{-}C_5H_4(CH{=}CH)_nC_7H_6)][PF_6]$[5a] on going from $n = 1$ to 3 there is a bathochromic shift of 1181 and 4305 cm^{-1} to the DA-CT and LL-CT bands respectively. By comparison, the same extension to the conjugated bridge results in a red-shift of magnitude 1720 and 2419 cm^{-1} to the DA-CT bands and 4069 and 4863 cm^{-1} to the LL-CT bands of the guaiazulenylium and azulenylium series respectively. This larger sequential lowering of the CT bands illustrates continued donor–acceptor interaction in the ground state even with increased π-bridge length.

As expected, the electron donating alkyl groups in the guaiazulenylium complexes stabilise the tropylium like cation making this moiety a weaker electron accepting group. This is reflected in a blue-shift of both CT bands in the guaiazulenylium series relative to the azulenylium derivatives with the exception of $n = 0$ which shows a subtle blue-shifted DA-CT transition for Fc-[0]-Az^+. It is obvious that with increasing *n* the difference in the λ_{max} values of the DA-CT transitions between the azulenylium and guaiazulenylium series increases which indicates a smaller BLA for the azulenylium complexes. A smaller BLA corresponds with a more diffuse charge in the azulene series revealing a lower dipole moment change upon excitation which is manifested in the reduced solvatochromism of this series.

Coordination of the $(RuCp)^+$ fragment is expected to generate a stronger dicationic electron-accepting terminus. However, both CT bands of Fc-[0]-Guaz$(RuCp)^{2+}$ are hypsochromically shifted relative to the monometallic complex as was the effect for the $(RuCp)^+$ coordinated and uncoordinated $[Fe(\eta^5\text{-}C_5H_5)(\eta^5\text{-}C_5H_4CH{=}CHC_7H_6)][PF_6]$[5a] complexes. This may be due to the increased contribution of the fulvene type resonance forms to the overall GS structure of the complex and it is certainly conceivable that they are electron rich enough for stable coordination of the metal fragment (Fig. 4). This can also be deduced from the electrochemistry data wherein the half wave potential of Fc-[0]-Guaz$(RuCp)^{2+}$ is more positively shifted relative to the $E_{\frac{1}{2}}$ value of Fc-[0]-Guaz$^+$. The apparent inconsistency between the blue shift of the CT transitions and the decrease of the difference between the oxidation and the reduction potentials when $[CpRu]^+$ is coordinated (see above) may be a consequence of the formation of additional filled and unfilled frontier orbitals upon coordination which gives rise to a change in their character and order. Therefore, the frontier orbitals involved in the ground and the excited states are expected to be different for Fc-[0]-Guaz$^+$ and Fc-[0]-Guaz$(RuCp)^{2+}$. Additionally, the MOs which are populated or depopulated during the electrochemical reduction and oxidation can be different from those related to the photochemical excitation.[16]

Hyperpolarisability measurements

Previous studies of sesquifulvalene complexes have indicated their potential as NLO candidates and therefore these complexes were subjected to hyper-Rayleigh scattering (HRS) studies.[17] The HRS experiments were carried out in CH_2Cl_2 at 1064 nm fundamental wavelength using *p*-nitroaniline (*p*NA) as an external reference. Concerning the two-level model (TLM) it is easily seen that the first hyperpolarisability (β) values of the compounds are resonance enhanced and therefore the static first hyperpolarisabilities (β_0) have been calculated using eqn. (1) (Table 4).[1] However, the TLM only takes into account the ground state and one excited state. Since the LL-CT transition demonstrate a dipole change between ground and the corresponding excited state indicated by the strong solvatochromic shift, it is expected that the LL-CT transition may also contribute to the first hyperpolarisability. Therefore the β_0 values in Table 4 should be taken with care. An intrinsic shortcoming of the HRS method arises when the energy of the frequency doubled radiation ($E_{2\omega}$) approaches the energy of the excited state (E_{eg}). Consecutively the CT state can be populated by the absorption of two photons, whereupon relaxation *via* fluorescence may affect the intensity of the HRS signal. As a result of the HRS method β will be overestimated due to this two-photon absorption fluorescence phenomenon (TPAF).[18] As the β values obtained were of such magnitude and the trends somewhat inconsistent, checks for TPAF were carried out.

Several techniques have been developed to avoid or abstract the TPAF contribution to β: long wavelength measurement,[19a–c] time resolved HRS,[19d] high frequency demodulation[19e] and measurement of the TPAF spectrum to abstract the fluorescence contribution to the HRS signal.[19f,g] A simpler methodology and the one used here is to introduce bandpass filters with peak transmittances at different wavelengths in front of the photomultiplier of the HRS set-up.[5a] A fluorescence signal should be considerably broader than the sharp HRS signal and the maximum of the emission band occurs only casually at $\lambda/2$.[19f,g] No TPAF enhancement was found for the complexes Fc-[0]-Az$^+$, Fc-[0]-Guaz$^+$ and Fc-[0]-Guaz$(RuCp)^{2+}$, however there is a contribution to the HRS signal of the longer π-bridge complexes (Fig. 6). It must also be stressed that we found this to be a purely qualitative test and therefore could not be used as a means to abstract the TPAF contribution.

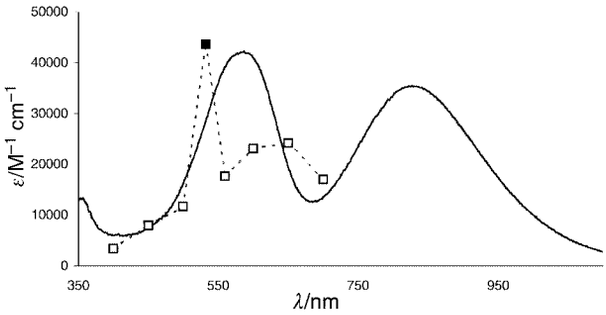

Fig. 6 Absorption (full) and emission (dotted) spectra of complex Fc-[3]-Guaz$^+$ in CH_2Cl_2; filled square is λ = 532 nm signal.

Further HRS examinations were carried out using long wavelength (1500 nm) laser excitation in an attempt to eliminate the complications experienced using the 1064 nm excitation wavelength. A tunable optical parametric oscillator (OPO)[20] based set-up was used to achieve the 1500 nm incident beam HRS examinations.[19a] For these complexes this technique was unsuccessful due to the high absorption of the complexes at $E_{2\omega}$ (750 nm) and the reduced sensitivity of the photomultiplier at $E_{2\omega}$.[21]

Additionally the chromophores Fc-[*n*]-Guaz$^+$ (n = 0–2) were subjected to a high frequency demodulation HRS examination using a fundamental wavelength of 1300 nm. The high frequency modulation of the fundamental beam enables us to distinguish between the time dependent fluorescence and the immediate hyper-Rayleigh scattering process.[19d] Only the Fc-[2]-Guaz$^+$ complex exhibited a measurable signal using this technique and hence we calculated a first hyperpolarisability of $\beta = 360 \times 10^{-30}$ esu. Again the observed signals were too low at higher frequencies due to the high absorptions of the complexes at 650 nm and instrumental demodulation. The hyperpolarisabilities measured by using the nanosecond 1064 nm laser are reported in Table 4.

As expected the determined β values of the non-fluorescent mononuclear complexes Fe-[0]-Az$^+$ and Fc-[0]-Guaz$^+$ increase in the order of electron-accepting strength: Az$^+$ > Guaz$^+$. The increase of the first hyperpolarisability with growing electron-accepting strength is also confirmed, when the mononuclear derivative Fc-[0]-Guaz is compared with the dicationic dinuclear complex Fc-[0]-Guaz$(RuCp)^{2+}$. Coupled with the interesting linear optical properties and the high air and photochemical stability of the chromophores, the results are nonetheless promising in that the relatively short donor–acceptor distances still yield quite high β values. Thus the concept of incorporating azulene and its alkylated derivatives as both electron donors and acceptors in potential NLO active compounds is still a profitable one. On the other hand the results also display the limited abilities of the available techniques in characterising the second order NLO potential especially of charged species.

Conclusion

We have presented a facile methodology towards the combination of the versatile and novel azulenic fragment with the ferrocene donor. Tuning of the electronic properties of the chromophores is made possible by modifying the length of the π linker as well as alkylation of and metal coordination to the azulenic fragment. X-Ray and electrochemical data for both series of complexes confirm the GS electronic interaction between the ferrocene and azulenylium based termini. This is less effective however in the case of the weaker electron accepting guaiazulenylium analogues and also upon π-bridge extension. Analysis of the linear and non-linear optical properties illustrates the potential of including both ferrocene and azulenic units in NLO research.

Experimental

Solvent purification and instrumentation

Dichloromethane, nitromethane and THF were dried by refluxing over calcium hydride and distilled prior to use. THF was further distilled from sodium–benzophenone. Acetonitrile was dried by refluxing over calcium hydride and distilled prior to use. Infrared spectra were recorded on a Perkin-Elmer Paragon 1000 spectrometer, UV-vis spectra on Perkin-Elmer Lambda 6 and 554 spectrometers and NMR spectra on JEOL JNM-GX 270 FT and Varian Geminin 200 BB spectrometers using $SiMe_4$ as an internal standard. Elemental analysis was carried out by the Microanalytical laboratory, University College, Dublin and the Institut für Anorganische und Angewandte Chemie, Universität Hamburg.

General procedure for condensation of ferrocenyl aldehydes with azulene and guaiazulene

An excess of HBF_4 (54% solution in diethyl ether) was added to an equimolar (1.6×10^{-4} M) solution of azulene or guaiazulene and a ferrocenyl aldehyde in THF (50 cm^3). The mixture was stirred for an hour at room temperature and then refrigerated overnight. The resulting precipitate was filtered off and washed well with diethyl ether.

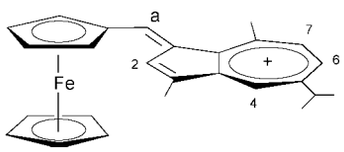

Fe-[0]-Guaz$^+$. Yield: 0.134 g (60%). δ_H (360 MHz; $(CD_3)_2CO$) 9.04 (1H, s, Ha), 8.70 (1H, d, $J_{4\text{-}6}$ 2.2, H4), 8.57 (1H, d, $J_{6\text{-}7}$ 11.2, H7), 8.40 (1H, dd, $J_{6\text{-}7}$ 11.1, $J_{6\text{-}4}$ 2.2 Hz, H6), 8.26 (1H, s, H2), 5.44 (2H, t, C_5H_4), 5.40 (2H, t, C_5H_4), 4.51 (5H, s, C_5H_5), 3.50 (4H, C8-Me, i-Pr CH), 2.58 (3H, s, C3-Me) and 1.48 (6H, d, J 6.88 Hz, i-Pr CH_3). δ_C (50 MHz; $(CD_3)_2CO$) 155.4 (**C**H=), 145.7, 143.8, 141.2, 139.7 (C7, C6, C2, C4), 88.9 (C_q of C_5H_4), 80.2, 75.2 (C_5H_4), 76.8 (C_5H_5), 39.8 (C8-Me), 28.7 ($CH(CH_3)_2$), 23.7 ($CH(CH_3)_2$) and 13.5 (C3-Me). λ_{max}/nm (ε/M^{-1} cm^{-1})-(CH_2Cl_2) 724 (13 517) and 474 (22 378); (CH_3CN) 700 (12 224) and 462 (21 233). Found: C 64.57, H 6.17. Calc. for $C_{26}H_{26}$-$BF_4Fe\cdot\frac{1}{2}$THF: C 64.90, H 6.03%.

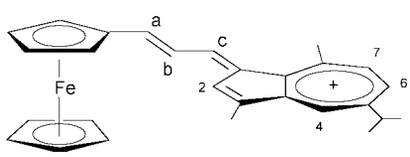

Fe-[1]-Guaz$^+$. Yield: 0.145 g (68%). δ_H (270 MHz; $(CD_3)_2CO$) 8.85 (1H, d, J 11.8, Hc), 8.70 (1H, d, $J_{4\text{-}6}$ 2.3, H4), 8.47 (2H, m, H6, H2), 8.38 (1H, dd, $J_{4\text{-}6}$ 2.3, $J_{6\text{-}7}$ 11.3, H6), 8.12 (1H, d, J 14.4, Ha), 7.81 (1H, dd, J 14.1, 11.8, Hb), 5.07 (4H, m, C_5H_4), 4.37 (5H, s, C_5H_5), 3.43 (4H, C8-Me, i-Pr CH), 2.61 (3H, s, C3-Me) and 1.48 (6H, d, J 0 7.03 Hz, i-Pr CH_3). δ_C (68 MHz; $(CD_3)_2CO$) 163.6, 161.6, 156.8, 155.7, 152.2, 149.5, 145.5, 143.3, 140.1, 139.7, 139.1, 135.3, 126.0 (Ca–Cc, C of Guaz), 82.8 (C_q of C_5H_4), 76.7, 72.0 (C_5H_4), 72.5 (C_5H_5), 39.6 (C8-Me), 27.3 ($CH(CH_3)_2$), 23.8 ($CH(CH_3)_2$) and 13.5 (C3-Me). λ_{max}/nm (ε/M^{-1} cm^{-1})(CH_2Cl_2) 782 (21 561) and 540 (31 767); (CH_3CN) 739 (19 591) and 513 (31 265). Found: C 65.72, H 5.94. Calc. for $C_{28}H_{28}BF_4Fe$: C 66.37, H 5.56%.

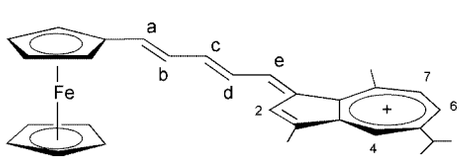

Fe-[2]-Guaz$^+$. Yield: 0.146 g (73%). δ_H (360 MHz; $(CD_3)_2CO$) 8.78 (1H, d, J 12.1, He), 8.73 (1H, d, J 1.9, H4), 8.47 (2H, m, H6, H7), 8.35 (1H, s, H2), 7.74 (1H, t, Hc), 7.56 (1H, t, Hd), 7.37 (1H, d, J 14.51, Ha), 6.98 (1H, t, Hb), 4.89 (4H, C_5H_4), 4.36 (5H, s, C_5H_5), 3.53 (1H, m, i-Pr CH), 3.43 (3H, s, C8-Me), 2.63 (3H, s, C3-Me) and 1.49 (6H, d, J 7.03 Hz, i-Pr CH_3). δ_C (68 MHz; $(CD_3)_2CO$) 165.8, 158.0, 156.3, 156.0, 151.8, 151.5, 150.1, 146.8, 143.7, 142.8, 139.4, 139.0, 137.9, 130.4, 129.2 (Ca–Cg, C of Guaz), 77.3, 74.8, 72.5 (Fc), 40.5 (C8-Me), 29.4 ($CH(CH_3)_2$), 24.2 ($CH(CH_3)_2$) and 13.7 (C3-Me). λ_{max}/nm (ε/M^{-1} cm^{-1})(CH_2Cl_2) 827 (35 394) and 587 (42 167); (CH_3CN) 760 (28 698) and 554 (35 391). Found: C 66.44, H 5.93. Calc. for $C_{30}H_{30}BF_4Fe\cdot\frac{1}{2}H_2O$: C 66.45, H 5.76%.

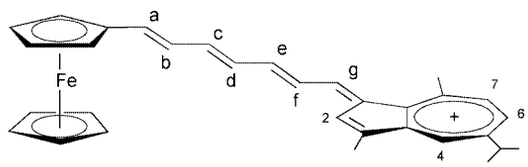

Fe-[3]-Guaz$^+$. Yield: 0.149 g (78%). δ_H (360 MHz; $(CD_3)_2CO$) 8.74 (2H, m, Hh, H4), 8.47 (2H, m, H6, H7), 7.72 (2H, m), 7.10 (2H, m), 6.87 (2H, m), 4.69 (2H, t, C_5H_4), 4.61 (2H, t, C_5H_4), 4.21 (5H, s, C_5H_5), 3.53 (1H, m, i-Pr CH), 3.44 (3H, s, C8-Me), 2.63 (3H, s, C3-Me) and 1.49 (6H, d, $CH(CH_3)_2$). No ^{13}C NMR due to solubility problems. λ_{max}/nm (ε/M^{-1} cm^{-1})(CH_2Cl_2) 859 (43 311) and 619 (43 641); (CH_3CN) 764 (34 062) and 594 (37 521). Found: C 66.66, H 5.89. Calc. for $C_{32}H_{32}BF_4Fe\cdot\frac{1}{2}$THF: C 68.49, H 6.39%.

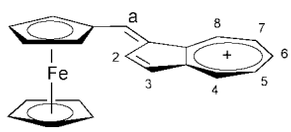

Fe-[0]-Az$^+$. Yield: 0.132 g (68%). δ_H (200 MHz; $(CD_3)_2CO$) 9.54 (1H, m, H8), 9.37 (1H, s, Ha), 8.99 (1H, m, H4), 8.60 (1H, d, J 5.1, H3), 8.53–8.43 (3H, m, H5, H6, H7), 7.93 (1H, d, J 4.9 Hz, H2), 5.81 (2H, t, C_5H_4), 5.56 (2H, t, C_5H_4) and 4.58 (5H, s, C_5H_5). δ_C (50 MHz; $(CD_3)_2CO$) 152.5 (Ca), 146.5, 138.7, 137.3 (C5, C6, C7), 143.6 (C4), 140.6 (C3), 140.5 (C8), 131.7 (C2), 83.9, 75.4 (C_5H_4) and 75.8 (C_5H_5). λ_{max}/nm (ε/M^{-1} cm^{-1})(CH_2Cl_2) 716 (10 174) and 474 (20 344); (CH_3CN) 699 (8 272) and 459 (12 311). Found: C 61.69, H 4.65. Calc. for $C_{21}H_{17}BF_4Fe$: C 61.22, H 4.16%.

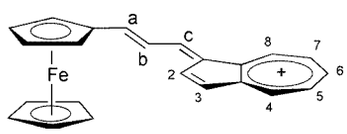

Fe-[1]-Az$^+$. Yield: 0.112 g (58%). δ_H (270 MHz; $(CD_3)_2CO$) 9.35 (1H, d, J 10.1, H8), 9.04 (1H, d, J 12.7, Hc), 8.97 (1H, d, J 9.0, H4), 8.75 (1H, d, J 4.8 Hz, H3), 8.45 (4H, m, Ha, H5, H6, H7), 7.89 (2H, m, Hb, H2), 5.47 (2H, t, C_5H_4), 5.28 (2H, t, C_5H_4) and 4.52 (5H, s, C_5H_5). δ_C (68 MHz; $(CD_3)_2CO$) 165.1, 150.6, 145.9, 143.1, 139.8, 139.7, 138.4, 136.9, 130.5, 126.4 (Ca–Cc, C2–C8), 155.5, 149.7, 134.1 (C_q of Az), 85.5 (C_q of C_5H_4), 80.7, 73.7 (C_5H_4) and 74.6 (C_5H_5). λ_{max}/nm (ε/M^{-1} cm^{-1})(CH_2Cl_2) 798 (17 301) and 552 (29 107); (CH_3CN) 762 (10 447) and 540 (15 082). Found: C 62.76, H 4.87. Calc. for $C_{23}H_{19}BF_4Fe$: C 63.06, H 4.37.

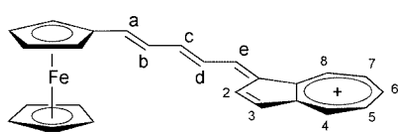

Fe-[2]-Az$^+$. Yield: 0.127 g (73%). δ_H (270 MHz; $(CD_3)_2CO$) 9.37 (1H, d, J 8.8, H8), 8.99 (1H, d, J 8.8, H4), 8.95 (1H, d,

J 12.8, He), 8.65 (1H, d, *J* 5.0, H3), 8.46 (3H, m, H5, H6, H7), 8.05 (1H, t, Hc), 7.89 (2H, dd, $J_{a\text{-}b}$ 14.3, $J_{2\text{-}3}$ 4.6, H2, Ha), 7.71 (1H, t, Hd), 7.14 (1H, dd, $J_{a\text{-}b}$ 14.3, $J_{b\text{-}c}$ 12.1 Hz, Hb), 5.16 (2H, t, C_5H_4), 5.02 (2H, t, C_5H_4) and 4.41 (5H, s, C_5H_5). δ_C (68 MHz; $(CD_3)_2CO$) 160.5, 158.2, 150.7, 145.8, 142.9, 139.7, 139.4, 138.9, 137.5, 130.9, 129.7, 128.9 (Ca–e, C2–8), 155.6, 149.7, 135.1 (C_q of Az), 84.3 (C_q of C_5H_4), 77.6, 72.1 (C_5H_4) and 73.2 (C_5H_5). λ_{max}/nm (ε/M^{-1} cm^{-1})(CH_2Cl_2) 866 (22 883) and 616 (31 143); (CH_3CN) 803 (17 324) and 595 (22 043). Found: C 64.55, H 5.19. Calc. for $C_{25}H_{21}BF_4Fe$: C 64.64, H 4.56%.

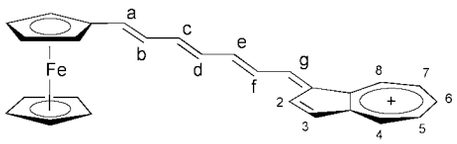

Fe-[3]-Az$^+$. Yield: 0.124 g (74%). δ_H (270 MHz; $(CD_3)_2CO$) 9.38 (1H, d, *J* 9.3, H8), 8.98 (1H, d, *J* 9.3, H4), 8.88 (1H, d, *J* 13.0, Hh), 8.65 (1H, d, *J* 5.1, H3), 8.45 (3H, m, H5, H6, H7), 8.01 (1H, t, olefinic H), 7.91 (1H, d, *J* 5.1, H2), 7.79 (1H, t, olefinic H), 7.54 (1H, t, olefinic H), 7.45 (1H, d, *J* 14.6 Hz, Ha), 6.95 (2H, m, olefinic H), 4.91 (2H, t, C_5H_4), 4.86 (2H, t, C_5H_4) and 4.32 (5H, s, C_5H_5). δ_C (68 MHz; $(CD_3)_2CO$) 160.8, 156.4, 154.6, 152.3, 150.5, 146.1, 143.2, 139.9, 138.3, 137.9, 137.8, 132.6, 131.5, 131.1, 128.7, 128.2 (Ca–Cg, C2–C8), 75.8, 71.2 (C_5H_4) and 72.5 (C_5H_5). λ_{max}/nm (ε/M^{-1} cm^{-1})(CH_2Cl_2) 920 (35 900) and 666 (34 909); (CH_3CN) 846 (26 315) and 628 (27 466). Found: C 65.07, H 4.85. Calc. for $C_{27}H_{23}BF_4Fe\cdot\frac{1}{2}H_2O$: C 64.91, H 4.81%.

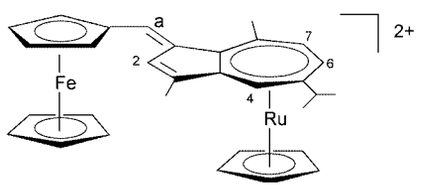

Reaction of Fc-[0]-Guaz$^+$ with [RuCp(MeCN)$_3$][PF$_6$]

A solution of [RuCp(MeCN)$_3$][PF$_6$] (0.08g, 0.18 mmol) in dry CH_2Cl_2 (10 cm^3) was added to a solution of [Fc-{0}-Guaz][PF$_6$] (0.1g, 0.19 mmol) in dry CH_2Cl_2 (10 cm^3). The mixture was stirred overnight and the volume then reduced to about 10 cm^3. The precipitate was filtered off and washed with dry Et_2O. Yield: 0.11 g (70%). ^{1}H NMR (CD_3NO_2, 200 MHz): δ 8.72 (1H, s, Ha), 8.03 (1H, s, H2), 7.71 (1H, s, H4), 7.39 (1H, d, $J_{6\text{-}7}$ 9.0, H7), 7.16 (1H, d, *J* 9.0, H6), 5.63 (5H, s, C_5H_5-Ru), 5.35, 5.30, 5.18, 5.07 (4H, s, C_5H_4), 4.33 (5H, s, C_5H_5), 3.39 (4H, C8-Me), 3.28 (1H, m, i-Pr CH), 2.39 (3H, s, C3-Me) and 1.42 (6H, d, *J* 6.9 Hz, i-Pr CH_3). ^{13}C NMR (CD_3NO_2, 50 MHz): δ 134.6 (CH=), 142.6, 101.0, 100.0, 94.25 (C7, C6, C2, C4), 89.32 (C_5H_4-Ru), 81.1, 80.7, 75.9, 75.2 (C_5H_4), 74.2 (C_5H_5), 38.2 (C8-Me), 29.6 ($CH(CH_3)_2$), 24.2, 23.2 ($CH(CH_3)_2$) and 13.0 (C3-Me). UV-vis (CH_2Cl_2): λ_{max}/nm (ε/M^{-1} cm^{-1}) 698 (17 152) and 462 (29 645); (CH_3CN) 688 (5 319) and 434 (17 722). Calc. for $C_{31}H_{31}F_{12}FeP_2Ru$: C 63.06, H 4.37. Found: C 62.47, H 6.68%.

Cyclic voltammetry

An Amel System 5000 was used. The measurements were performed in CH_2Cl_2 with 0.4 M [N(*n*-Bu)$_4$]ClO_4 as supporting electrolyte, *ca.* 10^{-3} M solutions of the complexes, a platinum wire as working electrode and a platinum plate (0.6 cm^2) as auxiliary electrode. The given potentials were measured against Ag–Ag^+ with a scan rate of 100 mV s^{-1} and are referenced against $E_{1/2}$([$FeCp_2$]–[$FeCp_2$]$^+$) = 0 V.

Crystal structure determinations

For Fc-[0]-Guaz$^+$ data collection was performed in *ca.* 8 hours using a fast Siemens axs CCD system as the compound was found to be X-ray sensitive and the structure solution calculated by direct methods with SHELXS 86.[22] The crystal structure shows disorder of the cationic ferrocenylguaiazulenylium moiety. About 13% of the molecules are replaced by their enantiomeric counterparts. The major form was refined (SHELXL 93)[23] with anisotropic thermal parameters with an idealised η^5-Cp ring that also shows 30% disorder (the carbon atoms of the minor form of the Cp ring were kept isotropic). Several restraints have been applied for the refinement of the minor form of the disordered ferrocenyl unit and only the iron atom was calculated with an anisotropic thermal parameter: the three five-membered rings in the molecule were idealized; several fixed bond lengths were applied (200 pm for Fe–C(η^5-Cp), 205 pm for Fe–C(η^5-C_5H_4) and 153 pm for sp^2–sp^3 and sp^3–sp^3 bonds); other C–C bonds (bridging atoms and seven-membered ring) were equalised to a length of *ca.* 140.6 pm. The highly disordered and therefore diffuse solvent molecule (THF) was only obtained to 60% of the expected electron density value. The C–O bonds as well as the C–C bonds were equalised.

Data collection for Fc-[0]-Guaz(RuCp)$^{2+}$ was performed on a Stoe IPDS diffractometer. The structure was solved by direct methods (SHELXS 86)[22] and refined with SHELXL 93.[23] Crystal data are given in Table 5.

CCDC reference number 186/2261.

See http://www.rsc.org/suppdata/dt/b0/b006624i/ for crystallographic files in .cif format.

Table 5 Crystal data and structure refinement for Fc-[0]-Guaz$^+$ and Fc-[0]-Guaz(RuCp)$^{2+}$

	Fc-[0]-Guaz(RuCp)$^{2+}$	**Fc**-[0]-Guaz$^+$
Chemical formula	$C_{31}H_{31}B_2F_8FeRu\cdot CH_3NO_2$	$C_{26}H_{26}BF_4Fe\cdot\frac{1}{2}C_4H_8O$
Formula weight	795.15	515.69
T/K	193	173
Crystal system	Monoclinic	Monoclinic
Space group	$P2_1/n$	$P2/n$
a/Å	15.5080(7)	11.2096(1)
b/Å	13.3829(8)	10.2163(2)
c/Å	16.0531(7)	22.1867(2)
β/°	96.94(5)	103.343(1)
V/Å^3	3307.3(3)	2472.25(6)
Z	4	4
μ/mm^{-1}	0.971	0.657
Collected reflections	24975	15381
Unique reflections	6223	5668
R_{int}	0.0703	0.0372
*R*1/*wR*2	0.0510/0.1272	0.0727/0.2098

HRS measurements of the first hyperpolarisabilities

Details for the experimental set-up can be found in ref. 16. A pulsed Nd:YAG laser with a wavelength of 1064 nm was used as incident light source. All measurements were carried out in dry CH_2Cl_2 with sample concentrations of 10^{-6} to 10^{-4} M using *p*-nitroaniline (*p*NA) as the external reference (β(*p*NA) = 21.6×10^{-30} esu).[17] The compounds were checked for fluorescence using the bandpass filter method described in refs. 5(*d*) and 13(*b*). Measurements at 1500 nm wavelength were carried out using a set-up similar to that described in ref. 18(*a*). Instead of the third harmonic (355 nm) generated from a Nd:YAG laser with a wavelength of 1064 nm the OPO[20] in use was pumped with the second harmonic (532 nm). The signal intensity at 824 nm and the fundamental at 532 nm were removed from the Idler using dichroic mirrors (HR 650 - 850 and HR 532), a green light and a silicon filter (transparent > 1000 nm). An additional Glan-Taylor polarizer ensured vertical polarisation of the beam into the measurement cell. Measurements were performed in CH_2Cl_2 with DR1 as the reference with a value of β_{1500} (DR1) = 59×10^{-30} esu. This value was obtained

by comparing the slopes of the reference in CH_2Cl_2 and $CHCl_3$ to obtain the ratio of β_{solute}.[24] Using the value $\beta(CHCl_3) = 66 \times 10^{-30}$ esu [19c] the hyperpolarisibility of DR1 (Disperse Red) in CH_2Cl_2 is estimated to be 59×10^{-30} esu. The effect of the refractive indices of the solvents was corrected using the simple Lorentz local field.[25] The high frequency demodulation experiments were performed as described in ref. 18(*e*). A Ti:sapphire laser was used to pump a femtosecond optical parametric oscillator, generating light of 1300 nm.[26] All solutions were prepared in CH_3CN and β values determined using DR1 as an external reference (β_{1300} (DR1) = 86×10^{-30} esu).

Acknowledgements

This work was supported by the European Union through TMR Network Contract No. ERBFMRX-CT98-0166. We would also like to thank Dr Falk Olbrich for the Fc-[0]-Guaz$^+$ crystallographic measurement and Degussa for the donation of $RuCl_3$.

References

1 J. L. Oudar and D. S. Chemla, *Chem. Phys.*, 1977, **66**, 2664; E. Hendrickx, K. Clays, A. Persoons, C. Dehu and J. L. Brédas, *J. Am. Chem. Soc.*, 1995, **117**, 3547.
2 J. Griffiths, in *Colour and Constitution of Organic Chemistry*, Academic Press, New York, 1976.
3 P. Suppan and N. Ghoneim, in *Solvatochromism*, The Royal Society of Chemistry, Cambridge, 1997.
4 D. R. Kanis, M. A. Ratner and T. J. Marks, *Chem. Rev.*, 1994, **94**, 195; N. J. Long, *Angew. Chem.*, 1995, **107**, 37; *Angew. Chem., Int. Ed. Engl.*, 1995, **34**, 21; H. S. Nalwa, *Appl. Organomet. Chem.*, 1991, **5**, 349; I. R. Whittall, A. M. McDonagh, M. G. Humphrey and M. Samoc, *Adv. Organomet. Chem.*, 1998, **42**, 291.
5 (*a*) H. Wong, T. Meyer-Friedrichsen, T. Farrell, C. Mecker and J. Heck, *Eur. J. Inorg. Chem.*, 2000, 631; (*b*) K. N. Jayaprakash, P. C. Ray, I. Matsuoka, M. M. Bhadbhade, V. G. Puranik, P. K. Das, H. Nishihara and A. Sarkar, *Organometallics*, 1999, **18**, 3851; (*c*) O. Briel, K. Sünkel, I. Krossing, H. Nöth, E. Schmälzlin, K. Meerholz, C. Braüchle and W. Beck, *Eur. J. Inorg. Chem.*, 1999, 483; (*d*) J. Mata, S. Uriel, E. Peris, R. Liusar, S. Houbrechts and A. Persoons, *J. Organomet. Chem.*, 1998, **562**, 197; (*e*) I. S. Lee, S. S. Lee, Y. K. Chung, D. Kim and N. W. Song, *Inorg. Chim. Acta*, 1998, **279**, 243.
6 C. Reichardt, in *Solvents and Solvent Effects in Organic Chemistry*, 2nd edn., VCH, Weinheim, 1988; M. Klessinger, *Chem. Unserer Zeit*, 1978, **12**, 1.
7 W. C. Hendron, *J. Phys. Chem.*, 1981, **85**, 3040.
8 A. E. Asato, R. S. H. Liu, V. P. Rao and Y. M. Cai, *Tetrahedron Lett.*, 1996, **37**, 419; G. Iftime and P. G. Lacroix, *Tetrahedron Lett.*, 1998, **39**, 6853; R. Herrmann, B. Pedersen, G. Wagner and J.-H. Youn, *J. Organomet. Chem.*, 1998, **571**, 261; J. N. Woodford, C. H. Wang, A. E. Asato and R. S. H. Liu, *J. Chem. Phys.*, 1999, **111**, 4621.
9 (*a*) C. W. Spangler and R. K. McCoy, *Synth. Commun.*, 1988, **18**, 51; (*b*) V. Alain, M. Blanchard-Desce, C.-T. Chen, S. R. Marder, A. Fort and M. Barzoukas, *Synth. Met.*, 1996, **81**, 133.
10 E. C. Kirby and D. H. Reid, *J. Chem. Soc.*, 1960, 494.
11 T. P. Gill and K. R. Mann, *Organometallics*, 1982, **1**, 485.
12 C.-T. Chen, S. R. Marder and L.-T. Cheng, *J. Chem. Soc., Chem. Commun.*, 1994, 259; S. R. Marder D. N. Beratan and L.-T. Cheng, *Science*, 1991, **252**, 103; S. R. Marder, B. Kippelen, A. K.-Y. Jen and N. Peyghambarian, *Nature* (*London*), 1997, **388**, 845; J.-L. Brédas, *Adv. Mater.*, 1995, **7**, 263.
13 (*a*) U. Behrens, *J. Organomet. Chem.*, 1979, **182**, 89; (*b*) J. Heck, S. Dabek, T. Meyer-Friedrichsen and H. Wong, *Coord. Chem. Rev.*, 1999, **190**, 1217.
14 S. R. Marder, J. W. Perry and B. G. Tiemann, *Organometallics*, 1991, **10**, 1896; V. Alain, M. Blanchard-Desce, C.-T. Chen, S. R. Marder, A. Fort and M. Barzoukas, *Synth. Met.*, 1996, 133; C. Lambert, W. Gaschler, M. Zabel, R. Matschiner and R. Wortmann, *J. Organomet. Chem.*, 1999, **592**, 109; T. J. J. Müller, A. Netz and M. Ansorge, *Organometallics*, 1999, **18**, 5066; J. A. Campo, M. Cano, J. V. Heras, C. Lopez-Garabito, E. Pinilla, R. Torres, G. Rojo and F. Agullo-lopez, *J. Mater. Chem.*, 1999, **9**, 899; B. J. Coe, C. J. Jones, J. A. McCleverty, D. Bloor and G. Cross, *J. Organomet. Chem.*, 1994, **464**, 225; A. Houlton, J. Naseralla, R. M. G. Roberts, J. Silver, D. Cunningham, P. McArdle and T. Higgins, *J. Chem. Soc., Dalton Trans.*, 1992, 2236; S. R. Marder, J. W. Perry, B. G. Tiemann and W. P. Schaefer, *Organometallics*, 1991, **10**, 1896.
15 (*a*) U. Hagenau, J. Heck, E. Hendrickx, A. Persoons, T. Schuld and H. Wong, *Inorg. Chem.*, 1996, **35**, 7863; (*b*) S. Barlow, H. E. Bunting, C. Ringham, J. C. Green, G. U. Bublitz, S. G. J. Boxer, W. Perry and S. R. Marder, *J. Am. Chem. Soc.*, 1999, **121**, 7227.
16 Preliminary DFT-MO calculations on archetypal sesquifulvalene complexes confirm this suggestion. The LL- and DA-CT transitions do not occur from this HOMO to the LUMO but from HOMO-3 and HOMO-1 to LUMO+2, respectively (M. Prosenc and J. Heck, in preparation).
17 K. Clays and A. Persoons, *Rev. Sci. Instrum.*, 1992, **63**, 3285.
18 (*a*) K. Clays, E. Hendrickx, T. Verbiest and A. Persoons, *Adv. Mater.*, 1998, **10**, 643; (*b*) J. J. Wolff and R. Wortmann, *J. Prakt. Chem.*, 1998, **340**, 99; (*c*) S. Stadler, G. Bourhill and C. Bräuchle, *J. Phys. Chem.*, 1996, **100**, 6927; (*d*) M. C. Flipse, R. De Jonge, R. H. Woudenberg, A. W. Marsman, C. A. Van Walree and L. W. Jenneskens, *Chem. Phys. Lett.*, 1995, **245**, 297.
19 (*a*) S. Stadler, R. Dietrich, G. Bourhill, C. Bräuchle, A. Pawlik and W. Grahn, *Chem. Phys. Lett.*, 1995, **247**, 271; (*b*) M. A. Pauley and C. H. Wang, *Rev. Sci. Instrum.*, 1999, **70**, 3285; (*c*) S. Stadler, R. Dietrich, G. Bourhill and C. Bräuchle, *Opt. Lett.*, 1996, **21**, 251; (*d*) O. F. J. Noordman and N. F. van Hulst, *Chem. Phys. Lett.*, 1996, **253**, 145; (*e*) G. Olbrechts, R. Strobbe, K. Clays and A. Persoons, *Rev. Sci. Instrum.*, 1998, **69**, 2233; (*f*) N. W. Song, T.-I. Kang, S. C. Jeoung, S.-J. Jeon, B. R. Cho and D. Kim, *Chem. Phys. Lett.*, 1996, **261**, 307; (*g*) O. K. Song, J. N. Woodford and C. H. Wang, *J. Phys. Chem. A*, 1997, **101**, 3222.
20 Paralite Optical Parametrical Oscillator, LAS GmbH.
21 Photomultiplier model 9863B/350, Electron Tubes Ltd.
22 G. M. Sheldrick, SHELXS 86, Program for crystal structure determination, University of Göttingen, 1986.
23 G. M. Sheldrick, SHELXL 93, Program for crystal structure refinement, University of Göttingen, 1993.
24 T. Kodaira, A. Watanabe, O. Ito, M. Matsuda, K. Clays and A. Persoons, *J. Chem. Soc., Faraday Trans.*, 1997, 3039.
25 K. Clays, A. Persoons and L. De Maeyer, *Adv. Chem. Phys.*, 1994, **85**, 455.
26 G. Olbrechts, K. Wostyn, K. Clays and A. Persoons, *Opt. Lett.*, 1999, **24**, 403.